JOURNAL OF GUIDANCE, CONTROL, AND DYNAMICS
Vol. 22, No. 2, March–April 1999

Autonomous Low-Earth-Orbit Determination from Magnetometer and Sun Sensor Data

Mark L. Psiaki*
Cornell University, Ithaca, New York 14853-7501

A batch filter has been designed to autonomously estimate the orbit of a spacecraft using only sensor data from an onboard magnetometer and sun sensor. The goal has been to prove the feasibility of a proposed low-cost, moderate-accuracy autonomous orbit determination system. The system uses a batch filter to estimate the Keplerian orbital parameters, a drag parameter, magnetometer biases, and corrections to the Earth's magnetic field. It does this by minimizing the square errors between measured and estimated values of two quantities, the Earth's magnetic field magnitude and the cosine of the angle between the sun vector and the Earth's magnetic field vector, both measured at the spacecraft. The proposed system is observable, and reasonable accuracy is obtainable. Given a magnetometer with a 10-nT 1-σ accuracy and a sun sensor with a 0.005-deg 1-σ accuracy, the system can achieve 1-σ position accuracies on the order of 500 m for inclined low Earth orbits.

I. Introduction

KNOWLEDGE of orbit and position is a requirement of virtually all spacecraft missions. There exist many orbit determination systems. Traditional systems rely on ground-based range and range-rate data to observe the orbit and position, as in Ref. 1. Autonomous orbit determination systems use only measurements that are available onboard a spacecraft. References 2–9 discuss various autonomous orbit determination schemes. The global positioning system (GPS) provides the possibility of a semiautonomous system. A spacecraft can determine its orbit solely from the positions and velocities that it gets from its GPS receiver. This is not truly autonomous because the spacecraft relies on signals from the GPS system. Furthermore, to get the best possible accuracy, differential GPS is needed, which relies on ground-based measurements as well.[10]

Different systems have widely different accuracy levels. Current ground-based systems can achieve position accuracies on the order of several centimeters.[1] GPS-based systems can have position accuracies ranging from about 100 m down to 0.1 m, depending on whether or not differential GPS is being employed or the GPS signal has been intentionally degraded for non-U.S.-military users.[2,10] The truly autonomous systems advertise various levels of accuracy, ranging from 50 km down to 1 km or better. Many such systems have been studied only via simulation; thus, their true accuracies are not yet known.

Even though GPS provides a low-cost and relatively accurate means of semiautonomous orbit determination, there is still a need for a truly autonomous orbit determination capability. Military satellites may need to be able to maintain orbit knowledge in the face of jamming, destruction of orbit determination infrastructure such as the GPS system, or both. Civilian satellites might not want to depend on GPS due to political reasons. A satellite program may not want to add the weight and power consumption of a GPS receiver if the spacecraft already has a compliment of sensors that can be used to determine its orbit.

The aims of the present work are to prove the observability of a new autonomous spacecraft orbit determination system and to estimate its likely accuracy. The new system can operate in a low Earth orbit (LEO). It uses only a 3-axes magnetometer and a sun sensor, both onboard the spacecraft. In addition to estimating the spacecraft's orbit, the system also estimates the magnetometer's biases and corrections to a model of the Earth's magnetic field.

The proposed system is the latest in a sequence of systems that base their orbit determination capability on measurements of the Earth's magnetic field.[4,6–9] The original idea, as introduced by Psiaki and Martel[4] and Psiaki et al.,[6] was to compare onboard measurements of the Earth's magnetic field magnitude with a spherical harmonic model of that field. Any deviations were used to correct the orbit parameters. Using various filter designs, this basic system has been tested on flight data by Psiaki et al.,[6] Shorshi and Bar-Itzhack,[8] and Wiegand.[9] Achieved steady-state accuracies in these studies ranged from 8 to 125 km. Accuracy was strongly influenced by the Earth field model's accuracy[6] and by field measurement accuracy.[6,8,9] Shorshi and Bar-Itzhack[8] also tested a system that uses attitude data. It achieved accuracies on the order of 10–35 km when tested with real flight data.[8]

Psiaki[7] attacked the problem of inaccuracy in the Earth field model by developing a system that estimates corrections to this model while estimating the spacecraft orbit. To make the orbit and field model coefficients simultaneously observable, this system included a 3-axes star sensor in addition to a 3-axes magnetometer. Simulation results predicted a system accuracy on the order of 300 m or better when using an accurate magnetometer and star sensor. If achievable in practice, this would be a dramatic accuracy gain over previous magnetometer-based systems, but the requirement of having an accurate 3-axes star sensor is a significant drawback of the system.

The present work is an extension of the work of Ref. 7. The new idea is to replace the 3-axes star sensor with a sun sensor. This would make the system much more economical. In fact, many missions already include a sun sensor and a magnetometer for attitude determination and control purposes. If the presently proposed system proved feasible, then it could be included on many missions at the cost of nothing more than some floating-point operations and memory in the flight computer.

There are three important questions in the present study. One is whether the spacecraft orbit and the magnetic field model coefficients remain simultaneously observable in a practical sense when only two axes worth of inertial attitude data are available; a sun sensor provides only two axes worth of data. If observability holds, then the other important questions are: What orbit/position accuracy might be achievable by such a system, and how does the achievable accuracy depend on orbit and system characteristics?

One might question why Earth horizon scanner data was not considered also. The reason is that inertial attitude information cannot be inferred from the Earth's horizon without prior knowledge of the orbit. Therefore, this type of data was deemed unlikely to aid in making the system fully observable. Despite its not having been

Received Dec. 1, 1997; presented as Paper 98-4308 at the AIAA Guidance, Navigation, and Control Conference, Boston, MA, Aug. 10–12, 1998; revision received Sept. 21, 1998; accepted for publication Sept. 30, 1998.

*Associate Professor, Sibley School of Mechanical and Aerospace Engineering. Associate Fellow AIAA.

considered, it must be admitted that incorporation of such data might further improve system accuracy.

An added benefit of the proposed system may accrue to the attitude determination system. The Earth's magnetic field is typically not as accurate an attitude reference as the sun or the Earth limb. This is due to field model uncertainty. If the presently proposed system proves successful, then its magnetic field model corrections could be used to improve the magnetic attitude reference. If the improvements were significant enough, then a horizon sensor might not be needed.

The present paper draws heavily on the methodology, models, and mathematics of Ref. 7. To conserve space, equations and models used in the present work will not be presented here if they can be found in that reference. Instead, the relevant equation number or section of that reference will be cited.

The remainder of this paper consists of five sections plus conclusions. Section II describes the batch filter that is used to estimate the orbit and the field model coefficients. The section describes the estimation vector, the orbital dynamics model, the measurement model, the least-squares technique used to solve the problem, and a statistical model of the filter's inputs and outputs. Section III describes covariance analysis and how it has been used to evaluate the proposed system. Section IV describes a truth model and how it has been used to test the filter. Section V discusses the results of the analyses that are defined in Secs. III and IV. Section VI discusses computational practicalities such as execution speed and convergence robustness. Section VII presents the conclusions.

II. Batch Filter Design

A. Estimation Vector

The batch filter estimates a vector of quantities that define the spacecraft orbit and corrections to the Earth's magnetic field model. Exactly as in Ref. 7, that vector is defined to be

$$\boldsymbol{p} = \Big[M_0, M_1, M_2, e, \omega_0, \lambda_0, i, b_x, b_y, b_z,\; q_1^0, q_1^1, s_1^1, \dot{q}_1^0, \dot{q}_1^1, \dot{s}_1^1, \dot{g}_1^0, \dot{g}_1^1, \dot{h}_1^1, \Delta g_1^0, \Delta g_1^1,\; \Delta h_1^1, \Delta g_2^0, \Delta g_2^1, \Delta h_2^1, \Delta g_2^2, \Delta h_2^2, \Delta g_3^0, \ldots, \Delta h_N^N\Big]^T \tag{1}$$

These estimated quantities can be broken down into three main categories: the components that define the orbit, elements 1–7; the magnetometer biases, elements 8–10; and the corrections to the Earth's magnetic field, elements 11 and up.

The orbital and magnetometer bias estimation parameters are defined as follows: M_0, M_1, e, ω_0, λ_0, and i are standard Kepler elements. They are, respectively, the mean anomaly at epoch, the mean motion at epoch, the eccentricity, the argument of perigee at epoch, the longitude of the ascending node at epoch, and the inclination. M_2 $(= \dot{M}_1/2)$ is not a standard Kepler element; it constitutes an approximate way to model one of the main effects of drag. The magnetometer biases are b_x, b_y, and b_z, all measured in spacecraft-fixed coordinates.

The field correction elements in $\boldsymbol{p}$ are 1) coefficients in a spherical harmonic expansion, 2) time rates of change of coefficients, or 3) perturbations of coefficients. The coefficients q_1^0, q_1^1, and s_1^1 are from a first-order external ring current model at epoch, and the corresponding rate terms, $\dot{q}_1^0$, $\dot{q}_1^1$, and $\dot{s}_1^1$, allow a constant time rate of change of the ring current, consistent with postmagnetic-storm field activity. The rate terms $\dot{g}_1^0$, $\dot{g}_1^1$, and $\dot{h}_1^1$ allow for an induced time variation of the first-degree coefficients of the internal field, which is consistent with the normal effects of an external ring current. The rest of the $\boldsymbol{p}$ vector's elements, $\Delta g_1^0, \ldots, \Delta h_N^N$, are coefficient perturbations. They account for uncertainty in the main internal spherical harmonic field model at epoch as given by some standard field model such as the International Geomagnetic Reference Field for a particular half decade.[11] These perturbations go up to Nth degree and Nth order.

The length of the estimated $\boldsymbol{p}$ vector is $(19 + N^2 + 2N)$. If $N = 10$ is used for the magnetic field model perturbations, then $\boldsymbol{p}$ has 139 elements. Many of the cases considered in Sec. V correspond to this size $\boldsymbol{p}$ vector.

B. Model of Orbital Motion

The batch filter uses a physics-based model of the orbital dynamics. It gives the geocentric position time history as a function of the Kepler elements at epoch and a drag parameter. The model takes the form

$$\theta = \theta(\Delta t; M_0, M_1, M_2, e, \omega_0, \lambda_0, i) \tag{2a}$$

$$\phi = \phi(\Delta t; M_0, M_1, M_2, e, \omega_0, \lambda_0, i) \tag{2b}$$

$$r = r(\Delta t; M_0, M_1, M_2, e, \omega_0, \lambda_0, i) \tag{2c}$$

where Δt is the time since epoch, θ colatitude, ϕ longitude, and r geocentric radius. This is the same model form as has been used in Ref. 7. Note that there is nothing special about using the Kepler elements at epoch as components of the estimation vector. Cartesian position and velocity at epoch could have been used in place of the Kepler elements.

Models of varying degrees of fidelity can be formally represented by the form of Eqs. (2a–2c). A high-fidelity model would use a number of terms in the spherical harmonic expansion of Earth's gravity field, an accurate atmospheric model, and solar and lunar gravity perturbations, to mention a few of the effects. These added complexities can be important when filtering actual flight data, but they are not important to the question of whether the system at hand is observable in a practical sense. Therefore, a relatively simple orbital model has been used. It only includes gravity terms out to the J_2 term, and even then only the secular J_2 effects are included. The drag model only includes the effects on altitude and mean motion. This simplified model is given in the Appendix of Ref. 7.

C. Model of Sensor Measurements

The sensors available to the system are a 3-axes magnetometer and a 2-axes sun sensor. In the discussion that follows, suppose that the measured magnetic field vector at sample time Δt_k is $\boldsymbol{B}_{\text{mes}(k)}$ and that the measured sun direction unit vector at the same sample instant is $\hat{\boldsymbol{s}}_{\text{mes}(k)}$, with both expressed in spacecraft coordinates.

Two Pseudomeasurements and Their Statistics

The measurements have been manipulated to yield pseudomeasurements that retain all of the position/orbit information of the original measurements but that are independent of spacecraft attitude. This independence allows decoupling of the attitude and orbit determination problems. The two useful pseudomeasurements are the measured magnitude of the Earth's magnetic field vector and the measured cosine of the angle between the Earth's magnetic field vector and the sun direction vector. The first pseudomeasurement is independent of attitude because the length of a vector does not depend on the particular coordinate system that is used to express its components. Similarly, the second pseudomeasurement is attitude independent because the angle between two vectors is independent of which common coordinate system is used to express their components.

The two pseudomeasurements can be expressed in terms of the actual measurements as follows:

$$y_{1\text{mes}(k)}(\boldsymbol{p}) = \sqrt{\left(\boldsymbol{B}_{\text{mes}(k)} - \boldsymbol{b}\right)^T \left(\boldsymbol{B}_{\text{mes}(k)} - \boldsymbol{b}\right)} \tag{3a}$$

$$y_{2\text{mes}(k)}(\boldsymbol{p}) = \frac{\hat{\boldsymbol{s}}_{\text{mes}(k)}^T \left(\boldsymbol{B}_{\text{mes}(k)} - \boldsymbol{b}\right)}{y_{1\text{mes}(k)}(\boldsymbol{p})} \tag{3b}$$

where $\boldsymbol{b} = [b_x, b_y, b_z]^T$ is the estimated magnetometer bias vector in spacecraft coordinates. Its inclusion in these formulas is why the pseudomeasurements depend on $\boldsymbol{p}$. The magnetic field magnitude $y_{1\text{mes}}$ is the same pseudomeasurement as was used in Ref. 6.

At times, the sun vector measurement $\hat{\boldsymbol{s}}_{\text{mes}(k)}$ may be unavailable. This could be caused by an eclipse of the sun by the Earth during part of the orbit. Alternatively, the spacecraft attitude may be such that the sun is outside of the field of view of the sun sensor. In either case, pseudomeasurement $y_{2\text{mes}(k)}$ will be unavailable.

Measurement error models for the pseudomeasurements can be derived from error models for the actual measurements. Suppose that the error models of the actual measurements are

$$\boldsymbol{B}_{\text{mes}(k)} = \boldsymbol{B}_{\text{act}(k)} + \boldsymbol{b} + \boldsymbol{n}_{B(k)} \tag{4a}$$

$$\hat{\boldsymbol{s}}_{\text{mes}(k)} = \hat{\boldsymbol{s}}_{\text{act}(k)} + \boldsymbol{n}_{s(k)} \tag{4b}$$

where $\boldsymbol{B}_{\text{act}(k)}$ is the actual magnetic field vector in spacecraft coordinates, $\hat{\boldsymbol{s}}_{\text{act}(k)}$ is the actual sun direction unit vector in spacecraft coordinates, and $\boldsymbol{n}_{B(k)}$ and $\boldsymbol{n}_{s(k)}$ are random, Gaussian, zero-mean, uncorrelated, discrete-time white noise measurement error vectors. All of these vectors correspond to sample time Δt_k. The statistics of the noise vectors are

$$E\{\boldsymbol{n}_{B(k)}\} = 0, \qquad E\{\boldsymbol{n}_{B(j)}\boldsymbol{n}_{B(k)}^T\} = \boldsymbol{I}\sigma_B^2\delta_{jk} \tag{5a}$$

$$E\{\boldsymbol{n}_{s(k)}\} = 0, \qquad E\{\boldsymbol{n}_{s(j)}\boldsymbol{n}_{s(k)}^T\} = \left(\boldsymbol{I} - \hat{\boldsymbol{s}}_{\text{act}(k)}\hat{\boldsymbol{s}}_{\text{act}(k)}^T\right)\sigma_s^2\delta_{jk} \tag{5b}$$

$$E\{\boldsymbol{n}_{B(j)}\boldsymbol{n}_{s(k)}^T\} = \boldsymbol{0} \tag{5c}$$

The term $(\boldsymbol{I} - \hat{\boldsymbol{s}}_{\text{act}(k)}\hat{\boldsymbol{s}}_{\text{act}(k)}^T)$ is included in Eq. (5b) so that, given the normalization $\hat{\boldsymbol{s}}_{\text{act}(k)}^T\hat{\boldsymbol{s}}_{\text{act}(k)} = 1$, $\boldsymbol{n}_{s(k)}$ will be perpendicular to $\hat{\boldsymbol{s}}_{\text{act}(k)}$, and $\hat{\boldsymbol{s}}_{\text{mes}(k)}$ will retain its normalization to first order in $\boldsymbol{n}_{s(k)}$. That $\boldsymbol{n}_{s(k)}$ is perpendicular to $\hat{\boldsymbol{s}}_{\text{act}(k)}$ is demonstrated by the argument

$$E\left\{\left(\hat{\boldsymbol{s}}_{\text{act}(k)}^T\boldsymbol{n}_{s(k)}\right)^2\right\} = E\left\{\hat{\boldsymbol{s}}_{\text{act}(k)}^T\boldsymbol{n}_{s(k)}\boldsymbol{n}_{s(k)}^T\hat{\boldsymbol{s}}_{\text{act}(k)}\right\}$$

$$= \hat{\boldsymbol{s}}_{\text{act}(k)}^T\left(\boldsymbol{I} - \hat{\boldsymbol{s}}_{\text{act}(k)}\hat{\boldsymbol{s}}_{\text{act}(k)}^T\right)\sigma_s^2\hat{\boldsymbol{s}}_{\text{act}(k)} = 0$$

This expectation value is zero if and only if $\hat{\boldsymbol{s}}_{\text{act}(k)}^T\boldsymbol{n}_{s(k)} = 0$. The normalization of $\hat{\boldsymbol{s}}_{\text{mes}(k)}$ to first order in $\boldsymbol{n}_{s(k)}$ is derivable as follows:

$$\hat{\boldsymbol{s}}_{\text{mes}(k)}^T\hat{\boldsymbol{s}}_{\text{mes}(k)} = \hat{\boldsymbol{s}}_{\text{act}(k)}^T\hat{\boldsymbol{s}}_{\text{act}(k)} + 2\hat{\boldsymbol{s}}_{\text{act}(k)}^T\boldsymbol{n}_{s(k)} + \boldsymbol{n}_{s(k)}^T\boldsymbol{n}_{s(k)} = 1 + \boldsymbol{n}_{s(k)}^T\boldsymbol{n}_{s(k)}$$

where the last result follows from the normalization of $\hat{\boldsymbol{s}}_{\text{act}(k)}$ and the orthogonality of $\boldsymbol{n}_{s(k)}$ and $\hat{\boldsymbol{s}}_{\text{act}(k)}$.

Note that the magnetometer model in Eq. (4a) includes only two types of errors, a bias and a Gaussian white-noise component. It has been suggested that a Markov process be included, if not in the filter, then at least in any truth model. The current model can be considered as the sum of two Markov processes, one with a very long correlation time and the other with a very short correlation time. The long correlation time is assumed to be longer than the batch interval, which translates the slow process into an effective bias. The short correlation time is assumed to be shorter than the sample interval, which makes the fast process look like white noise to the filter. Lacking sufficient knowledge of the characteristics of a specific magnetometer, it was deemed unnecessary, at this point of the work, to include a Markov process with an intermediate correlation time.

The noise model for the pseudomeasurements is derived using Eqs. (3a–4b). First, one substitutes Eqs. (4a) and (4b) into Eqs. (3a) and (3b) and forms Taylor series expansions in terms of the noise vectors $\boldsymbol{n}_{B(k)}$ and $\boldsymbol{n}_{s(k)}$. The resulting equations are

$$y_{1\text{mes}(k)} = \sqrt{\boldsymbol{B}_{\text{act}(k)}^T\boldsymbol{B}_{\text{act}(k)}} + \frac{\boldsymbol{B}_{\text{act}(k)}^T\boldsymbol{n}_{B(k)}}{\sqrt{\boldsymbol{B}_{\text{act}(k)}^T\boldsymbol{B}_{\text{act}(k)}}} + \mathcal{O}\left(\boldsymbol{n}_{B(k)}^2\right) \tag{6a}$$

$$y_{2\text{mes}(k)} = \frac{\hat{\boldsymbol{s}}_{\text{act}(k)}^T\boldsymbol{B}_{\text{act}(k)}}{\sqrt{\boldsymbol{B}_{\text{act}(k)}^T\boldsymbol{B}_{\text{act}(k)}}} + \frac{\boldsymbol{B}_{\text{act}(k)}^T\boldsymbol{n}_{s(k)}}{\sqrt{\boldsymbol{B}_{\text{act}(k)}^T\boldsymbol{B}_{\text{act}(k)}}} + \frac{\hat{\boldsymbol{s}}_{\text{act}(k)}^T}{\sqrt{\boldsymbol{B}_{\text{act}(k)}^T\boldsymbol{B}_{\text{act}(k)}}}$$

$$\times\left[\boldsymbol{I} - \frac{\boldsymbol{B}_{\text{act}(k)}\boldsymbol{B}_{\text{act}(k)}^T}{\boldsymbol{B}_{\text{act}(k)}^T\boldsymbol{B}_{\text{act}(k)}}\right]\boldsymbol{n}_{B(k)} + \mathcal{O}\left(\boldsymbol{n}_{s(k)}^2, \boldsymbol{n}_{s(k)}\boldsymbol{n}_{B(k)}, \boldsymbol{n}_{B(k)}^2\right) \tag{6b}$$

If one neglects the higher-order terms in $\boldsymbol{n}_{B(k)}$ and $\boldsymbol{n}_{s(k)}$, then these equations can be rewritten in the form

$$y_{1\text{mes}(k)} = y_{1\text{act}(k)} + n_{y1(k)} \tag{7a}$$

$$y_{2\text{mes}(k)} = y_{2\text{act}(k)} + n_{y2(k)} \tag{7b}$$

where $y_{1\text{act}(k)}$ is defined as the first term on the right-hand side of Eq. (6a), $n_{y1(k)}$ is defined as the second term on the right-hand side of Eq. (6a), $y_{2\text{act}(k)}$ is defined as the first term on the right-hand side of Eq. (6b), and $n_{y2(k)}$ is defined as the sum of the second and third terms on the right-hand side of Eq. (6b). These definitions of the error terms, coupled with the statistical models of $\boldsymbol{n}_{B(k)}$ and $\boldsymbol{n}_{s(k)}$ in Eqs. (5a–5c), can be used to deduce the following statistical models for $n_{y1(k)}$ and $n_{y2(k)}$:

$$E\{n_{y1(k)}\} = 0, \qquad E\{n_{y1(j)}n_{y1(k)}\} = \sigma_B^2\delta_{jk} \tag{8a}$$

$$E\{n_{y2(k)}\} = 0 \tag{8b}$$

$$E\{n_{y2(j)}n_{y2(k)}\} = \left[1 - \frac{\left(\hat{\boldsymbol{s}}_{\text{act}(k)}^T\boldsymbol{B}_{\text{act}(k)}\right)^2}{\boldsymbol{B}_{\text{act}(k)}^T\boldsymbol{B}_{\text{act}(k)}}\right]\left[\sigma_s^2 + \frac{\sigma_B^2}{\boldsymbol{B}_{\text{act}(k)}^T\boldsymbol{B}_{\text{act}(k)}}\right]\delta_{jk}$$

$$E\{n_{y1(j)}n_{y2(k)}\} = 0 \tag{8c}$$

Thus, the two pseudomeasurements have errors that are statistically uncorrelated. Strictly speaking, these results are valid only in the limit of small measurement noise because linearizations were used to derive them.

It is helpful to redefine the standard deviation for $n_{y2(k)}$ as

$$\sigma_{y2(k)} = \sqrt{\left[1 - \frac{\left(\hat{\boldsymbol{s}}_{\text{mes}(k)}^T\boldsymbol{B}_{\text{mes}(k)}\right)^2}{\boldsymbol{B}_{\text{mes}(k)}^T\boldsymbol{B}_{\text{mes}(k)}}\right]\left[\sigma_s^2 + \frac{\sigma_B^2}{\boldsymbol{B}_{\text{mes}(k)}^T\boldsymbol{B}_{\text{mes}(k)}}\right]} \tag{9}$$

This differs slightly from Eq. (8b), but the difference is not significant if the measurement errors and biases are relatively small. The standard deviation definition in Eq. (9) is preferable to the original one given in terms of $\boldsymbol{B}_{\text{act}(k)}$ and $\hat{\boldsymbol{s}}_{\text{act}(k)}$ because the latter quantities are never known exactly.

Models of the Pseudomeasurements

The filter needs a model of what the measurements should be for a given value of its estimated $\boldsymbol{p}$ vector. This section defines that model.

The measurement model makes use of a spherical harmonic expansion of the Earth's magnetic field. The functional form of this spherical harmonic model is

$$\boldsymbol{B}_{\text{sez}}(\theta, \phi, r; \boldsymbol{p}, \Delta t) = \begin{bmatrix} B_\theta(\theta, \phi, r; \boldsymbol{p}, \Delta t) \\ B_\phi(\theta, \phi, r; \boldsymbol{p}, \Delta t) \\ B_r(\theta, \phi, r; \boldsymbol{p}, \Delta t) \end{bmatrix} \tag{10}$$

where $\boldsymbol{B}_{\text{sez}}(\theta, \phi, r; \boldsymbol{p}, \Delta t)$ is expressed in local south–east–zenith coordinates. The exact form of this model is given in Eqs. (3a–3c) of Ref. 7. As denoted in Eq. (10), the field depends on the geocentric position, (θ, ϕ, r), and on the field model coefficients and coefficient perturbations in the $\boldsymbol{p}$ estimation vector. $\boldsymbol{B}_{\text{sez}}$ depends directly on time because of the field model coefficient rate terms, $\dot{q}_1^0, \dot{q}_1^1, \dot{s}_1^1, \dot{g}_1^0, \dot{g}_1^1$, and $\dot{h}_1^1$.

Note that the standard time dependence of $\boldsymbol{B}_{\text{sez}}$, found in Ref. 11, has been omitted. The standard time dependence is used to correct five-year reference fields for predicted field drift that occurs over the course of several years. In the current filter these effects are taken into account by direct estimation of field model coefficient corrections, thus obviating the need for the usual drift terms in the model.

The function $\boldsymbol{B}_{\text{sez}}(\theta, \phi, r; \boldsymbol{p}, \Delta t)$ can be used to compute the modeled value of the first pseudomeasurement as a function of the estimation vector and the sample time:

$$y_{1\text{mod}}(\Delta t_k; \boldsymbol{p}) = \sqrt{\boldsymbol{B}^T_{\text{sez}}[\theta(\Delta t_k, \boldsymbol{p}), \phi(\Delta t_k, \boldsymbol{p}), r(\Delta t_k, \boldsymbol{p}); \boldsymbol{p}, \Delta t_k]\, \boldsymbol{B}_{\text{sez}}[\theta(\Delta t_k, \boldsymbol{p}), \phi(\Delta t_k, \boldsymbol{p}), r(\Delta t_k, \boldsymbol{p}); \boldsymbol{p}, \Delta t_k]} \tag{11}$$

The dependence of θ, ϕ, and r on Δt_k and $\boldsymbol{p}$ has been explicitly presented in this formula to completely express the dependence of $y_{1\text{mod}}$ on these two quantities.

The model for the y_2 dependence on Δt_k and $\boldsymbol{p}$ can be derived in inertial coordinates. Define the inertial coordinate system, also called the celestial coordinate system, as having its $+x$ axis in the equatorial plane and pointing toward the first point of Aries, its $+z$ axis along the north pole, and its $+y$ axis defined by the right-hand rule. The transformation from local south–east–zenith coordinates to celestial coordinates takes the functional form $\boldsymbol{A}_{\text{cc/sez}}(\gamma_0, \theta, \phi, \Delta t)$, where γ_0 is the Greenwich hour angle at epoch. Given this transformation and the sun unit vector in celestial coordinates at sample instant k, $\hat{\boldsymbol{s}}_{\text{cc}(k)}$, the model for the second pseudomeasurement becomes

$$y_{2\text{mod}}(\Delta t_k; \boldsymbol{p}) = \frac{\hat{\boldsymbol{s}}^T_{\text{cc}(k)}\, \boldsymbol{A}_{\text{cc/sez}}[\gamma_0, \theta(\Delta t_k, \boldsymbol{p}), \phi(\Delta t_k, \boldsymbol{p}), \Delta t_k]\, \boldsymbol{B}_{\text{sez}}[\theta(\Delta t_k, \boldsymbol{p}), \phi(\Delta t_k, \boldsymbol{p}), r(\Delta t_k, \boldsymbol{p}); \boldsymbol{p}, \Delta t_k]}{y_{1\text{mod}}(\Delta t_k; \boldsymbol{p})} \tag{12}$$

(As defined here, the vector $\hat{\boldsymbol{s}}_{\text{cc}(k)}$ depends only on time. For very precise sun sensor measurements (on the order of 0.0037 deg for the highest altitude orbits considered), this vector's dependence on spacecraft position also would need to be considered if filtering actual flight data. This need arises due to the parallax effect. Neglect of solar parallax has little impact on the present simulation study, except to make its results slightly more conservative for very accurate sun sensor measurements.)

D. Error Equations, Nonlinear Least-Squares Estimator, and Statistical Interpretation

The goal of the batch filter is to choose the $\boldsymbol{p}$ estimation vector that best matches the pseudomeasurements to their modeled values. Mathematically this leads to the following system of error equations:

$$e_{1(k)} = \frac{1}{\sigma_B}\Big[y_{1\text{mod}}(\Delta t_k; \boldsymbol{p}) - y_{1\text{mes}(k)}(\boldsymbol{p})\Big], \quad \text{for} \quad k = 1, \ldots, N \tag{13a}$$

$$e_{2(k)} = \frac{1}{\sigma_{y2(k)}}\Big[y_{2\text{mod}}(\Delta t_k; \boldsymbol{p}) - y_{2\text{mes}(k)}(\boldsymbol{p})\Big]$$

$$\text{for all} \quad k = 1, \ldots, N \text{ such that (s.t.) } \hat{\boldsymbol{s}}_{\text{mes}(k)} \text{ is available} \tag{13b}$$

where N is the number of samples in the batch. These equations have been scaled using the standard deviations for $n_{y1(k)}$ and $n_{y2(k)}$ to normalize the standard deviations of the pseudomeasurement errors $e_{1(k)}$ and $e_{2(k)}$.

The batch filter estimates $\boldsymbol{p}$ by computing the value that minimizes the sum of the square errors from Eqs. (13a) and (13b). In other words, the estimate of $\boldsymbol{p}$ minimizes

$$J(\boldsymbol{p}) = \frac{1}{2}\sum_{k=1}^{N}\left[\frac{y_{1\text{mod}}(\Delta t_k; \boldsymbol{p}) - y_{1\text{mes}(k)}(\boldsymbol{p})}{\sigma_B}\right]^2 + \frac{1}{2}\sum_{k \text{ s.t. } \hat{\boldsymbol{s}}_{\text{mes}(k)} \text{avail.}}\left[\frac{y_{2\text{mod}}(\Delta t_k; \boldsymbol{p}) - y_{2\text{mes}(k)}(\boldsymbol{p})}{\sigma_{y2(k)}}\right]^2 \tag{14}$$

where this cost function uses the definitions of $y_{1\text{mes}(k)}(\boldsymbol{p})$ and $y_{2\text{mes}(k)}(\boldsymbol{p})$ given by Eqs. (3a) and (3b) and the definitions of $y_{1\text{mod}}(\Delta t_k; \boldsymbol{p})$ and $y_{2\text{mod}}(\Delta t_k; \boldsymbol{p})$ given by Eqs. (11) and (12).

The filter solves this nonlinear least-squares problem via an iterative numerical technique. Each iteration uses the Gauss–Newton method to compute a tentative search step, $\Delta \boldsymbol{p}$. Next, it performs a line search to choose a step-length rescaling, α, that approximately minimizes $J(\boldsymbol{p} + \alpha\, \Delta \boldsymbol{p})$, subject to the constraints $0 < \alpha \leq 1$. If the nonlinearities are not strong or if the iterations are near a solution with low residual errors, then $\alpha = 1$ will be a good scaling because $\Delta \boldsymbol{p}$ is the solution of a linearized least-squares problem. For other situations, an α in the range $0 < \alpha < 1$ will be chosen because there always exists an α in this range that achieves $J(\boldsymbol{p} + \alpha\, \Delta \boldsymbol{p}) < J(\boldsymbol{p})$. The iterations repeat until it becomes impossible to make further significant decreases in $J(\boldsymbol{p})$. Reference 12 gives the details of this and related numerical algorithms on pp. 133–141.

The filter needs to compute the partial derivatives with respect to $\boldsymbol{p}$ of $y_{1\text{mes}(k)}(\boldsymbol{p})$, $y_{2\text{mes}(k)}(\boldsymbol{p})$, $y_{1\text{mod}}(\Delta t_k; \boldsymbol{p})$, and $y_{2\text{mod}}(\Delta t_k; \boldsymbol{p})$. These are needed to solve for $\Delta \boldsymbol{p}$ in the Gauss–Newton nonlinear least-square solution procedure and to infer the error statistics of the $\boldsymbol{p}$ estimate. The needed partial derivatives are

$$\frac{\partial y_{1\text{mes}(k)}}{\partial \boldsymbol{p}} = \left[-\left(\boldsymbol{B}_{\text{mes}(k)} - \boldsymbol{b}\right)^T \frac{\partial \boldsymbol{b}}{\partial \boldsymbol{p}} \Big/ y_{1\text{mes}(k)}\right] \tag{15a}$$

$$\frac{\partial y_{2\text{mes}(k)}}{\partial \boldsymbol{p}} = -\left[\hat{\boldsymbol{s}}^T_{\text{mes}(k)} \frac{\partial \boldsymbol{b}}{\partial \boldsymbol{p}} \Big/ y_{1\text{mes}(k)}\right] - \left[\frac{y_{2\text{mes}(k)}}{y_{1\text{mes}(k)}}\right] \frac{\partial y_{1\text{mes}(k)}}{\partial \boldsymbol{p}} \tag{15b}$$

$$\frac{\partial y_{1\text{mod}(k)}}{\partial \boldsymbol{p}} = \boldsymbol{B}^T_{\text{sez}}\left(\frac{\partial \boldsymbol{B}_{\text{sez}}}{\partial \theta}\frac{\partial \theta}{\partial \boldsymbol{p}} + \frac{\partial \boldsymbol{B}_{\text{sez}}}{\partial \phi}\frac{\partial \phi}{\partial \boldsymbol{p}} + \frac{\partial \boldsymbol{B}_{\text{sez}}}{\partial r}\frac{\partial r}{\partial \boldsymbol{p}} + \frac{\partial \boldsymbol{B}_{\text{sez}}}{\partial \boldsymbol{p}}\right) \Big/ y_{1\text{mod}(k)} \tag{15c}$$

$$\frac{\partial y_{2\text{mod}(k)}}{\partial \boldsymbol{p}} = \hat{\boldsymbol{s}}^T_{\text{cc}(k)}\left[\left(\frac{\partial \boldsymbol{A}_{\text{cc/sez}}}{\partial \theta}\boldsymbol{B}_{\text{sez}} + \boldsymbol{A}_{\text{cc/sez}}\frac{\partial \boldsymbol{B}_{\text{sez}}}{\partial \theta}\right)\frac{\partial \theta}{\partial \boldsymbol{p}} + \left(\frac{\partial \boldsymbol{A}_{\text{cc/sez}}}{\partial \phi}\boldsymbol{B}_{\text{sez}} + \boldsymbol{A}_{\text{cc/sez}}\frac{\partial \boldsymbol{B}_{\text{sez}}}{\partial \phi}\right)\frac{\partial \phi}{\partial \boldsymbol{p}} + \boldsymbol{A}_{\text{cc/sez}}\left(\frac{\partial \boldsymbol{B}_{\text{sez}}}{\partial r}\frac{\partial r}{\partial \boldsymbol{p}} + \frac{\partial \boldsymbol{B}_{\text{sez}}}{\partial \boldsymbol{p}}\right)\right] \Big/ y_{1\text{mod}(k)} - \left[\frac{y_{2\text{mod}(k)}}{y_{1\text{mod}(k)}}\right]\frac{\partial y_{1\text{mod}(k)}}{\partial \boldsymbol{p}} \tag{15d}$$

Note that the matrix $\partial \boldsymbol{b}/\partial \boldsymbol{p}$ is a matrix with three rows. It is mostly zeros except for three entries with a value of 1 because the elements of $\boldsymbol{b}$ constitute three of the elements of $\boldsymbol{p}$, see Eq. (1).

Linearized versions of Eqs. (13a) and (13b) can be used to infer the statistics of the error in the estimate of $\boldsymbol{p}$. Linearized about the estimated solution, $\hat{\boldsymbol{p}}$, the error equations take the form

$$\begin{bmatrix} e_{1(1)} \\ \vdots \\ e_{1(N)} \\ e_{2(1)} \\ \vdots \\ e_{2(N)} \end{bmatrix} = \boldsymbol{A}(\boldsymbol{p}_{\text{act}} - \hat{\boldsymbol{p}}) \tag{16a}$$

with

$$\boldsymbol{A} = \begin{bmatrix} \frac{1}{\sigma_B}\left(\frac{\partial y_{1\text{mod}(1)}}{\partial \boldsymbol{p}} - \frac{\partial y_{1\text{mes}(1)}}{\partial \boldsymbol{p}}\right) \\ \vdots \\ \frac{1}{\sigma_B}\left(\frac{\partial y_{1\text{mod}(N)}}{\partial \boldsymbol{p}} - \frac{\partial y_{1\text{mes}(N)}}{\partial \boldsymbol{p}}\right) \\ \frac{1}{\sigma_{y2(1)}}\left(\frac{\partial y_{2\text{mod}(1)}}{\partial \boldsymbol{p}} - \frac{\partial y_{2\text{mes}(1)}}{\partial \boldsymbol{p}}\right) \\ \vdots \\ \frac{1}{\sigma_{y2(N)}}\left(\frac{\partial y_{2\text{mod}(N)}}{\partial \boldsymbol{p}} - \frac{\partial y_{2\text{mes}(N)}}{\partial \boldsymbol{p}}\right) \end{bmatrix} \tag{16b}$$

where $\boldsymbol{A}$ is the Jacobian matrix of Eqs. (13a) and (13b) evaluated at $\hat{\boldsymbol{p}}$ and where $\boldsymbol{p}_{\text{act}}$ is the true value of $\boldsymbol{p}$. Note that the y_2 rows are omitted for sample times that lack sun sensor data.

The linearized estimate of the error covariance is

$$\boldsymbol{P}_p = E\left\{(\boldsymbol{p}_{\text{act}} - \hat{\boldsymbol{p}})(\boldsymbol{p}_{\text{act}} - \hat{\boldsymbol{p}})^T\right\} = (\boldsymbol{A}^T\boldsymbol{A})^{-1} \tag{17}$$

This follows because the $e_{i(j)}$ errors have zero mean and unit variance and because $\hat{\boldsymbol{p}}$ has been derived by minimizing the sum of the square errors in the equations. The zero-mean and unit-variance properties of the $e_{i(j)}$ errors are consequences of these errors' definitions in Eqs. (13a) and (13b), coupled with the measurement and statistical noise models in Eqs. (7a–9).

III. Covariance Analysis and Practical Observability

Observability of the system is equivalent to uniqueness of the minimum of the least-squares cost function $J(\boldsymbol{p})$. Because this is a nonlinear problem, the only practical observability test that can be applied is a local one. A sufficient condition for a unique local minimum of $J(\boldsymbol{p})$ is that the Hessian matrix, $\mathrm{d}^2J/\mathrm{d}\boldsymbol{p}^2$, be positive definite (Ref. 12, pp. 63–65). The measurement residuals, i.e., the remaining errors at the minimum, are normally very small; therefore, it can be shown that $\mathrm{d}^2J/\mathrm{d}\boldsymbol{p}^2 \cong \boldsymbol{A}^T\boldsymbol{A}$ (Ref. 12, p. 134). The matrix $\boldsymbol{A}^T\boldsymbol{A}$ is the observability Gramian for a linearized discrete-time model of this system.[13] Because $\boldsymbol{A}^T\boldsymbol{A}$ is a squared matrix, it is positive definite if and only if it is nonsingular. Thus, observability of this system can be proved by proving that the matrix $\boldsymbol{A}^T\boldsymbol{A}$ is nonsingular.

Practical observability depends on the distance of $\boldsymbol{A}^T\boldsymbol{A}$ away from singularity. Distance is a relative notion that changes with problem scaling. Therefore, a better measure of observability is the error covariance of the estimated vector $\boldsymbol{P}_p = (\boldsymbol{A}^T\boldsymbol{A})^{-1}$. If the standard deviations, the square roots of the diagonals of $\boldsymbol{P}_p$, are small in a problem-dependent sense, then the system is practically observable. Therefore, the standard deviations of the magnetometer biases and of the magnetic field model corrections will be used as practical measures of these quantities' observability.

Actual spacecraft position standard deviations are better measures of practical orbit observability than are the standard deviations of the Kepler elements and the drag term. The spacecraft's instantaneous position standard deviation can be inferred from $\boldsymbol{P}_p$, in a linearized sense, via application of the chain rule and of the definition of covariance. Equations (11) and (12) of Ref. 7 give a method for inferring the along-track/cross-track/altitude covariance matrix at a particular time as a function of $\boldsymbol{P}_p$ and $\hat{\boldsymbol{p}}$. Three good measures of practical orbit observability are the maxima, taken over the batch time interval, of the standard deviations of the three position error components.

IV. Testing Against a Simulated Truth Model

A. Comparison of Filter Outputs with Truth Model Values

The proposed system has been studied using simulated data from a truth model. The truth model contains dynamics, measurements, and sensor noise. It produces simulated magnetometer and sun sensor data. This data is generated by using truth values for the Kepler elements, the drag parameter, the magnetometer biases, and the field model coefficients, which constitute a truth value of the estimation vector $\boldsymbol{p}_{\text{truth}}$. The simulated output data is then fed into the filter, which produces an estimate of the truth model's orbit and field.

Filter performance can be evaluated by comparing the truth model's orbit and field to the filter's estimate of these quantities. Individual cases can be compared, or statistical comparisons can be made via Monte Carlo analysis. The present study uses only individual case comparisons. All of the statistical processes that are considered can be analyzed via covariance analysis, which has been described already. Therefore, Monte Carlo analysis, with its computational burden, is not needed. Comparison of individual cases reveals the amount of error that is caused by the systematic effects, which are considered in the present study.

Several types of comparisons are made between truth model values and the filter output. The estimated orbit is compared with the truth model orbit in terms of along-track, cross-track, and altitude error as observed in the local coordinate system attached to the truth-model spacecraft position. These errors are determined from an analysis that uses the truth-model values and the estimated values of the Kepler elements and the drag parameter. The magnetometer biases and the field model coefficient perturbations are compared directly. Additionally, the inertial direction of the estimated magnetic field at the estimated spacecraft location is compared with the inertial direction of the truth-model magnetic field at the truth-model spacecraft location.

B. Truth Models of Orbit and Attitude Dynamics

The truth model of the orbital dynamics uses the same model as is used in the filter. The truth model uses the truth values of the Kepler elements M_0, M_1, e, ω_0, λ_0, and i and the truth value of the drag parameter M_2. These are given in the $\boldsymbol{p}_{\text{truth}}$ vector. These values are input to Eqs. (2a–2c) to generate the truth-model spacecraft position time history.

Often, a truth model's dynamics will include random process noise, a more accurate physical model than the filter's dynamic model, or both. This is done to test whether the filter's proposed dynamic model is sufficiently accurate to achieve the projected performance. In the present case, it is assumed that it would be possible to incorporate a sufficiently accurate dynamic model into the filter, as the research in Ref. 1 suggests, so that dynamic model fidelity limitations would not significantly impact filter accuracy for real flight data. Because of this assumption, time and effort has not been devoted to development of a truth model that could explore this issue. Of course, the validity of this assumption will need to be evaluated in the future by testing the filter with real flight data.

The filter's pseudomeasurements are independent of attitude, yet the spacecraft's attitude dynamics might affect the observability of the system and, therefore, the accuracy of the filter. The spacecraft attitude affects the orientation of the spacecraft-fixed magnetometer axes with respect to the field and with respect to the sun vector. The estimated magnetometer biases are defined along these axes; therefore, their observability might be affected by the attitude time history of the spacecraft. Also, the sun is detected by a sun sensor onboard the spacecraft. Sun sensors normally have a limited field of view. Depending on the attitude time history, the sun might be outside of that field of view some of the time, which means that sun measurements would not be available at those times.

Two different types of attitude time history have been used in the truth model. One is for a nadir-pointing spacecraft. In this model one axis of the spacecraft body is always pointing along (negative)

orbit normal, one is nominally pointing toward nadir, and the other is nominally pointing along the velocity vector. The other attitude dynamics model is that of a spin-stabilized spacecraft. In this case the spin axis is assumed to be sun pointing. Both attitude dynamics models produce a transformation from celestial coordinates to spacecraft coordinates, $\boldsymbol{A}_{sc/cc}(\Delta t)$, that is a function of time.

C. Truth Models of Measurements

Each truth-model magnetometer measurement is constructed by a multistep process. First, the truth model spacecraft position coordinates θ_k, ϕ_k, and r_k are computed for sample time Δt_k by substituting Δt_k and the $\boldsymbol{p}_{\text{truth}}$ Kepler elements and drag parameter into Eqs. (2a–2c). Next, these position components, Δt_k, and $\boldsymbol{p}_{\text{truth}}$ are input into Eq. (10) to determine the truth value of the field in south–east–zenith coordinates, $\boldsymbol{B}_{sez(k)}$. Third, the values θ_k and ϕ_k, the Greenwich hour angle at epoch γ_0, and the sample time Δt_k are used to compute the truth value of the transformation from local south–east–zenith coordinates to celestial coordinates, $\boldsymbol{A}_{cc/sez(k)}$. Next, this transformation is used with the truth-model attitude transformation at time Δt_k, $\boldsymbol{A}_{sc/cc(k)}$, to transform $\boldsymbol{B}_{sez(k)}$ into spacecraft coordinates: $\boldsymbol{B}_{sc(k)} = \boldsymbol{A}_{sc/cc(k)}\boldsymbol{A}_{cc/sez(k)}\boldsymbol{B}_{sez(k)}$. Finally, a random noise vector and the truth values of the magnetometer bias vector are added to $\boldsymbol{B}_{sc(k)}$ to yield the truth-model magnetometer measurement vector: $\boldsymbol{B}_{mes(k)} = \boldsymbol{B}_{sc(k)} + \boldsymbol{b}_{\text{truth}} + \boldsymbol{n}_{B(k)}$, where $\boldsymbol{n}_{B(k)}$ is the random vector whose statistics are defined in Eq. (5a).

There are two types of errors between the truth model magnetic field and the filter's initial guess of the Earth's magnetic field. First, $\boldsymbol{B}_{sez}$ is affected by the truth values of the field model coefficient perturbations contained in $\boldsymbol{p}_{\text{truth}}$. Second, the truth magnetic field model may contain terms beyond those of the filter. For many cases considered, the filter used a 10th-degree, 10th-order field model, but the truth model used a 13th-degree, 13th-order model. This addition of higher-order terms to the spherical harmonic model of the field constitutes a systematic error between the truth model and the filter.

The truth model of the sun sensor measurements includes noise and considers eclipse by the Earth and the finite width of the sun sensor field of view. The truth model first computes the spacecraft's Cartesian position in inertial coordinates by using the truth quantities r_k and $\boldsymbol{A}_{cc/sez(k)}$. This position and the sun direction vector in celestial coordinates, $\hat{\boldsymbol{s}}_{cc(k)}$, are used to determine whether or not the sun is visible or eclipsed by the Earth. If visible, then the sun measurement vector is computed by using the truth model spacecraft attitude to calculate $\hat{\boldsymbol{s}}_{sc(k)} = \boldsymbol{A}_{sc/cc(k)}\hat{\boldsymbol{s}}_{cc(k)}$ and a random noise vector to determine $\hat{\boldsymbol{s}}_{mes(k)} = (\hat{\boldsymbol{s}}_{sc(k)} + \boldsymbol{n}_{s(k)})/\|\hat{\boldsymbol{s}}_{sc(k)} + \boldsymbol{n}_{s(k)}\|$. The statistics of $\boldsymbol{n}_{s(k)}$ are defined by Eq. (5b) with $\hat{\boldsymbol{s}}_{act(k)}$ replaced by $\hat{\boldsymbol{s}}_{sc(k)}$ in that equation's covariance definition. Once $\hat{\boldsymbol{s}}_{mes(k)}$ has been computed, the truth model checks whether it falls within the field of view of the sun sensor, which is defined by a center-of-field vector in spacecraft coordinates and by a field radius in degrees. If $\hat{\boldsymbol{s}}_{mes(k)}$ falls within this field of view, then it is recorded as a measurement; otherwise, no sun sensor measurement is recorded.

V. Results

A. Covariance-Based Practical Observability of Various Cases

The system has proved observable in many important cases. It is theoretically observable in all situations except that of an orbit with zero inclination and zero eccentricity. It is practically observable in most situations that are sufficiently far away from having zero inclination and zero eccentricity. These results are like those presented in Ref. 7, where there was 3-axes star sensor data available to the batch filter.

The dependence of system estimation standard deviations on orbit parameters has been extensively investigated. A sequence of cases has been considered, all of which respect the following set of assumptions: The filter estimates coefficient corrections for a 10th-degree, 10th-order field model. The spacecraft is spinning with a spin period of 50.235 s and is sun pointed. The magnetometer accuracy is 10-nT 1-σ for the random white noise component; the biases can be much larger because they get estimated. The sun sensor accuracy is 0.005-deg 1-σ, and this error source is primarily random white noise. The intersample interval is $\Delta t_k - \Delta t_{k-1} = 60$ s, and the total number of samples is $N = 1441$; this means that each batch contains one full day's worth of data. The relationship between the sun's inertial direction and the longitude of the orbit's ascending node is such that the spacecraft can experience eclipse. The eclipse may be as much as 37% of the orbit for some inclinations and orbital altitudes.

Various estimation error standard deviations for these cases are presented in Table 1 as functions of orbital parameters. The second through fourth columns of Table 1 give the orbital characteristics for the case, inclination, apogee height, and perigee height. The next three columns give the maximum position standard deviations during the batch interval, where A-T stands for along track and C-T for cross-track. The eighth column gives the maximum of the standard deviations of the three first-degree field model coefficient corrections, Δg_1^0, Δg_1^1, and Δh_1^1. The last column gives the maximum of the standard deviations of the three magnetometer biases, b_x, b_y, and b_z.

Table 1 demonstrates the effect of inclination, eccentricity, and altitude on observability. Practical observability decreases with inclination as evidenced by cases 1–5. All five of the tabulated standard deviations increase as inclination decreases. Observability decreases with increased altitude, as evidenced by cases 2 and 7. Eccentricity helps observability. Otherwise, the standard deviations of case 8, which has a very low inclination but significant eccentricity, would have been much higher.

These results are similar to what was found in Ref. 7, where data from a 3-axes star sensor were assumed to be available to the filter. One would expect the results in Ref. 7 to be at least as good as the present results. This is generally the case, but the results in Ref. 7 are better only by a factor of about 2 or less. The present results are remarkable because they derive from one axis less of attitude data and from an attitude sensor that is less accurate by a factor of 9. (There is one axis less of attitude data because Ref. 7 assumed the availability of 3-axes star sensor data, but the current study assumes that attitude data is available only from a sun sensor. The spacecraft's rotation about the sun vector is the lost component of orientation information. The measured magnetic field vector does not provide a third axis of attitude information for purposes of orbit determination because the field model and its inertial direction remain uncertain until after the filter has found its solution.)

As an illustration of the types of results that the covariance analysis produces, Fig. 1 presents three time histories of position component estimation error standard deviations. These plots correspond to case 2 in Table 1. The epoch time for this case corresponds to the start of the batch interval, which occurs at $\Delta t = 0$ in Fig. 1. Recall that these standard deviations are inferred by propagating

Table 1 Orbit, field coefficient, and bias standard deviations as functions of orbital parameters

Case	i, deg	Apogee altitude, km	Perigee altitude, km	Max. component σ			Max. σ of 1st-deg field, nT	Max. σ of magnet. bias, nT
				A-T, m	C-T, m	Altitude, m		
1	88.1	585	515	379	206	90	1.9	0.7
2	75.0	585	515	415	250	98	2.0	0.7
3	45.0	585	515	560	381	116	6.3	1.2
4	30.0	585	515	761	579	149	38.4	1.7
5	15.0	585	515	1326	1160	216	1.29×10^3	2.1
6	75.0	3200	500	607	616	178	2.9	0.7
7	75.0	3200	3100	1531	1214	405	6.6	0.9
8	1.0	3200	500	4410	3724	531	1.43×10^4	1.0

Table 2 Orbit, field coefficient, and bias standard deviations as functions of sun sensor accuracy

Case	σ_s, deg	Max. component σ			Max. σ of 1st-deg field, nT	Max. σ of magnet. bias, nT
		A-T, m	C-T, m	Altitude, m		
1	0.0005	404	244	97	2.0	0.7
2	0.005	415	250	98	2.0	0.7
3	0.05	795	498	198	3.9	1.1
4	0.25	1396	2104	404	8.8	1.6

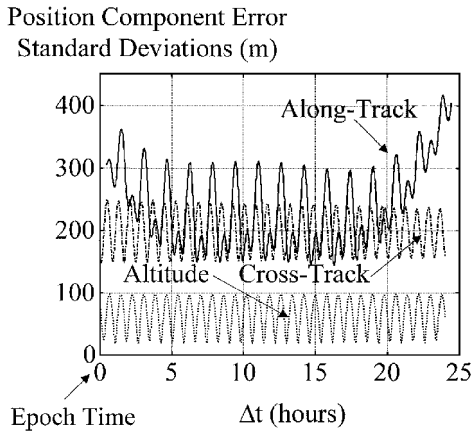

Fig. 1 Time histories of estimation-error standard deviations of three position components for a representative case.

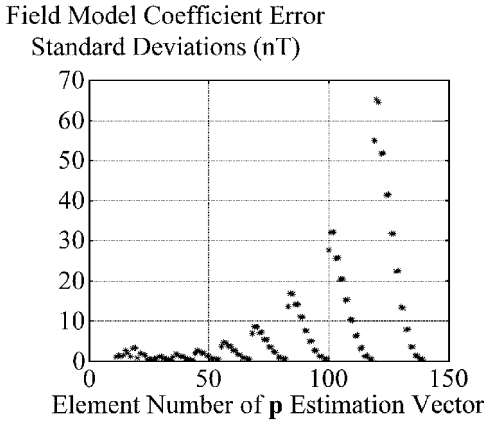

Fig. 2 Standard deviations of estimation errors of field model coefficients for a representative case.

the covariances of the Kepler elements through various (linearized) geometric transformations. The data in columns 5–7 of Table 1 are the maximum values of each of these three curves, maximized over the batch interval. One can see that the along-track standard deviation has a secular component. This is the result of uncertainty in the estimated orbital period and drag term.

Figure 2 presents the standard deviations of the field coefficient errors in an estimated $\boldsymbol{p}$ vector. These particular covariance results correspond to case 2 of Table 1. These standard deviations are for elements 11–139 of $\boldsymbol{p}$. The standard deviations are plotted vs the element number; i.e., Fig. 2 plots $\sqrt{(\boldsymbol{p}_p)_{jj}}$ vs j for $j = 11$–139 $(= \dim\{\boldsymbol{p}\})$. The secular rate standard deviations (the σ associated with, e.g., $\dot{q}_1^0$ and $\dot{g}_1^1$) have been multiplied by the batch duration $(\Delta t_N - \Delta t_1)$ before being plotted; this gives their effects in nanotesla at the end of the interval.

The point of Fig. 2 is to show the accuracy with which the various field model corrections can be estimated by the batch filter. As can be seen, this filter's ability to estimate field perturbations is good for low spherical harmonic degrees, but field correction accuracy degrades for higher degrees. Recall from Eq. (1) that the spherical harmonic degree of the correction terms increases as the element number of the $\boldsymbol{p}$ estimation vector increases. This decrease in field model accuracy with increased degree is different from the results of Ref. 7. In that study, if inclination and eccentricity were not too close to zero, then the field model coefficients could be estimated accurately for all degrees and orders in the model.

The effect of the availability of the sun has also been investigated. Another case has been run that is like case 2 in Table 1. The only difference is that the sun is never in eclipse behind the Earth. For this case the three maximum standard deviations of the position error components are 781-m along track, 138-m across track, and 158 m in altitude. This is surprising. Intuition suggests that the availability of more data should increase accuracy, but along-track and altitude accuracy actually decrease. Presumably, this is an effect of the change in geometry between the orbit normal vector and the sun observation vector.

Another variable that is related to sun availability is the type of attitude dynamics that the spacecraft has. A nadir-pointing spacecraft with a limited sun sensor field of view will collect less sun direction data than a properly designed sun-pointing spin-stabilized spacecraft. This study considered a nadir-pointing spacecraft model with a 128-deg-diam sun sensor field of view. It consistently achieved poorer position error standard deviations than the spin-stabilized, sun-pointing spacecraft. For the nadir-pointing spacecraft in an orbit like that of case 2 in Table 1, the filter's maximum position standard deviations are: 908-m along track, 319-m across track, and 352 m in altitude, which is obviously worse than the sun-pointing case that is given in Table 1. This comparison typifies many other cases: position standard deviations can increase by factors as large as 4 when going to a nadir-pointing spacecraft with a 128-deg-diam sun sensor field of view. It has not been determined whether or not this effect has more to do with the geometry of the magnetometer bias estimates or with the change in the amount of available sun sensor data, but the latter is suspected to be the case.

The sensors' accuracies have a direct impact on the filter's predicted standard deviations. It is obvious that more accurate sensors would yield lower predicted standard deviations, but the relative effects of the two sensors' standard deviations is less obvious. A series of cases has been run, each of which is like case 2 of Table 1 except that the sun sensor accuracy σ_s has been varied. The results are given in Table 2. Table 2 shows that the nominal sun sensor accuracy of $\sigma_s = 0.005$ deg is well matched with the magnetometer accuracy that has been used for all of these cases, $\sigma_B = 10$ nT. More sun sensor accuracy yields very little position accuracy improvement, but less sun sensor accuracy degrades the filter's performance.

The length of the filtering interval affects the position accuracy. A case has been run that is like case 1 of Table 1, except that the time between samples has been lengthened from 60 to 120 s. This means that two days' worth of data are used instead of one day's worth. The maximum position standard deviations for this case are: 262-m along track, 204-m across track, and 86 m in altitude. This represents a 31% reduction in the peak along-track standard deviation. The other two standard deviations are reduced only modestly. This along-track accuracy improvement can be traced to increased accuracy of the estimates of the Kepler elements M_0 and M_1 and draglike parameter M_2.

To illustrate the usefulness of the proposed system, a simulation of a typical spacecraft case has been run. This case was designed to correspond to the ALEXIS spacecraft mission as much as possible.[14] The nominal ALEXIS orbit has an apogee of 830 km, a perigee of 740 km, and an inclination of 70 deg. The ALEXIS fine sun sensor has an advertised accuracy of 0.05 deg. A magnetometer accuracy of 10 nT was assumed for this case to increase the

likelihood of achieving good results. ALEXIS is a spin-stabilized spacecraft whose spin axis points (roughly) toward the sun. The batch filter used one day's worth of simulated data sampled at 60-s intervals, as in most other cases considered here. The maximum position standard deviations achieved for this case were: 899-m along track, 570-m across track, and 224 m in altitude. These standard deviations place the 3-σ position accuracy well within the 5-km specification that was set for orbit knowledge on this mission. If ALEXIS had been equipped with an accurate magnetometer and if its spacecraft-generated fields had been well calibrated, then the proposed system might have been able to serve as ALEXIS' primary orbit determination system.

B. Comparisons with Truth Model Outputs

Various issues have been investigated by filtering data from the truth model and comparing the filter's estimated $\boldsymbol{p}$ vector with the truth value of $\boldsymbol{p}$. Although true Monte Carlo analysis has not been done, truth model comparisons have been used to verify, in an approximate manner, the results of the covariance analysis. In all cases where only random errors were present, the highest ratio of an actual error to a precomputed standard deviation was 2.48. Thus, the 3-σ rule, when applied using the predicted standard deviations from the covariance analysis, proved sufficient to bound the worst-case errors.

The effect of truncation of the field model has been investigated by truth-model/filter comparison. Four different filters have been considered, all operating on data from a simulated orbit like that of case 2 in Table 1. Each used a 10th-degree, 10th-order model of the Earth's magnetic field, but each estimated corrections for a different number of the coefficients in its field model. One estimated corrections only up to the 7th degree and 7th order, another up to 8th degree and 8th order, a third up to 9th degree and 9th order, and the fourth estimated corrections for all of the coefficients up to 10th degree and 10th order. The truth model's field was a 13th-degree/13th-order spherical harmonic model. Thus, it differed from each of the filters' models for the 11th–13th degree and order terms. For the lower-order terms, the truth model had random errors between its coefficients and the filters' a priori coefficients. These random errors had a normal distribution with a standard deviation of 1% of the nominal coefficient value. The filters were not given a model of these error sources. Random magnetometer and sun sensor errors were included, but their standard deviations, $\sigma_B = 0.1$ nT and $\sigma_s = 5 \times 10^{-5}$ deg, were small enough to make their effects negligible.

Omission of higher-degree field-model correction estimates does not significantly affect orbit determination accuracy. For example, the maximum along-track errors between the filters' estimated orbits and the truth-model orbits were 328, 381, 378, and 319 m for the four respective filters, i.e., for the 7th-, 8th-, 9th-, and 10th-degree and -order filters. The results are similar for the other position error components' peak values. Thus, the filter's position error is not degraded seriously if field model corrections are estimated only up to 7th degree and 7th order.

This result is consistent with Fig. 2, which shows that the filter does a poorer job of estimating higher-degree and higher-order field model coefficient corrections. It stands to reason that if the filter cannot estimate a quantity very accurately then it will not do much worse if it uses an a priori estimate for that quantity. A reduction to 7th-degree and 7th-order corrections greatly reduces the number of elements in the $\boldsymbol{p}$ estimation vector, from 139 to 82. This reduction speeds computer execution times and reduces memory requirements.

There is a possible side benefit to simultaneous orbit and magnetic field model estimation. This benefit is an improvement of the modeled inertial direction of the Earth's magnetic field. Using currently available models of the Earth's magnetic field, the field model's local inertial direction may be wrong by as much as 0.4 deg or more, assuming a 300-nT field error and a 40,000-nT field strength. In each of the comparisons with the truth model, the estimated and truth-model inertial directions of the Earth's magnetic field have been compared. The results are very encouraging. For simulations corresponding to the cases listed in Table 1 and with a 13th-degree/13-order truth field model, the maximum inertial direction error of the estimated field was 0.11 deg. If cases 5 and 8 had been eliminated because of their poorer general observability due to low inclination, then the maximum inertial direction error of the field would have been just 0.08 deg. Similar accuracy has been achieved by filters that estimate field model coefficient corrections only up to the 7th degree and 7th order.

This field direction accuracy opens up the possibility of changing standard attitude determination systems. These improved field model accuracies are comparable to those of standard Earth limb detectors.[14] Therefore, it might be possible to fly a spacecraft with only a magnetometer and a sun sensor. These two sensors could be used to estimate both orbit and attitude. The attitude estimate could be accurate to better than 0.1 deg on all three axes. Of course, this analysis presupposes a spacecraft with an accurate magnetometer that is remote from sources of large unmodeled spacecraft-generated fields.

C. Comparisons with Simplified Filters

Comparisons with simpler filters have been carried out to determine how the current filter achieves improvements. In comparison to the filter in Ref. 6, the current filter adds two features: the inclusion of sun sensor data and the estimation of field model coefficient corrections. Reference 8 found that inclusion of attitude data alone can improve some aspects of filter performance. Therefore, there is a question about the current filter: how much of its accuracy improvement comes from adding sun sensor data and how much comes from estimating field model coefficients?

This question has been answered by filtering truth-model data using two simplified filters. One filter was the same as described earlier, except that it did not estimate any field model coefficient perturbations. In this case the length of the $\boldsymbol{p}$ estimation vector was only 10. In the second case, the filter was further simplified by discarding the sun sensor measurements so that the y_2 pseudomeasurement was not used. This latter filter was equivalent to the batch filter of Ref. 6. In both of these cases the truth model had a 13th-degree/13th-order field, and the filter used a 10th-degree/10th-order field. Where applicable, the filter's field model coefficients were set to be different than the corresponding coefficients of the truth model. These differences were random and normally distributed and had a standard deviation equal to 1% of the nominal coefficient's magnitude. To account for the increased uncertainty in the Earth's field, the value of σ_B was increased to 200 nT in both filters. The cases that were run corresponded to the orbital conditions of case 1 in Table 1.

Both simplified filters showed significantly poorer performance than the filter that has been developed in this paper. The first filter, the one that used sun sensor data without estimating field model corrections, had the following peak position errors: 7600-m along track, 2300-m across track, and 1100 m in altitude. The filter that used only magnetometer measurements did even worse. Its peak position errors were: 13,100-m along track, 14,800-m across track, and 800 m in altitude.

These results show that the addition of attitude data reduces the total position error by a factor of about 2. The attitude data produces its largest improvement in the determination of the orbital plane, which yields better cross-track accuracy. This is roughly the same as what was found in Ref. 8 for the gamma ray observatory spacecraft.

These results show that it is important to add field model coefficient corrections to the filter's estimation vector. To see this, compare the results for case 1 of Table 1 with the preceding results that use sun sensor measurements but no estimation of field model corrections. Suppose that the predicted maximum errors are three times as large as the standard deviations listed in case 1 of Table 1, i.e., assume 3-σ limits. Then, for the simulation case considered in this section, the elimination of field coefficient corrections increased the maximum position component errors by factors ranging from 3.7 to 6.7, and the total position error was increased by a factor of about 6.7.

VI. Computational Issues

The issues of computer memory requirements, required computation time, and convergence robustness are important to consider

as gauges of the proposed filter's practicality. All experience reported here is for runs on a 100-MHz Pentium using Fortran. The memory requirements depend on the size of the $\boldsymbol{p}$ estimation vector. Care has been taken to use memory in an efficient manner by processing data recursively in small batches rather than in one large batch. Double precision variables have been used throughout. The filter's executable program and data storage occupied the following amounts of memory: 544 kbytes for 10th-degree/10th-order field model corrections, 475 kbytes for 9th-degree/9th-order corrections, 419 kbytes for 8th-degree/8th-order corrections, and 374 kbytes for 7th-degree/7th-order corrections.

The solution speed depends on the dimension of the $\boldsymbol{p}$ estimation vector and on the accuracy of the first guess. It makes the most sense to talk about the execution time per major Gauss–Newton iteration. The problem would be solvable in just one such iteration if it were linear. Multiple iterations are required to minimize the nonlinear least-squares cost function. The computation time per iteration was 56 s per iteration for the filter with 10th-degree/10th-order field model corrections, 37 s for the filter with 9th-degree/9th-order corrections, 27 s for the 8th-degree/8th-order filter, and 21 s for the 7th-degree/7th-order filter.

The number of Gauss–Newton iterations required to solve for the estimate from a given set of data depended on the goodness of the initial guesses of the orbit, the magnetometer biases, and the field model. Almost all runs were started with random initial errors in the biases between ± 300 nT and with random field model coefficient errors distributed normally with a standard deviation of 1% of the nominal coefficient value. Typical runs had initial rms total position errors in the range 160–310 km and converged in 3–13 Gauss–Newton iterations. The worst initial position error for which successful convergence was achieved was 1420-km rms. This case took 9 Gauss–Newton iterations to converge. One case with an rms initial position error of 560 km took 20 Gauss–Newton iterations to converge. Convergence was slowed by an ad-hoc feature of the least-squares solver that limited absolute step sizes in hopes of avoiding convergence to erroneous local minima.

Convergence robustness has been demonstrated by the ability to converge from 1400-km rms initial position error. This is about as good as the convergence that was obtained in Ref. 8. Computational experience indicates that convergence from larger initial errors probably is feasible if the orbit parameterization is changed from Keplerian elements to something that does not have singularities. The Kepler singularities, such as the one at zero eccentricity, can cause there to be multiple local minima of the least-squares cost function.

VII. Conclusions

A batch filter has been designed to estimate the orbit of an LEO spacecraft, and its performance has been analyzed. The only sensor data that this filter needs are the measurements from a 3-axes magnetometer and from a sun sensor, both onboard the spacecraft. The filter also estimates the magnetometer's biases and corrections to a spherical harmonic model of the Earth's magnetic field.

The position accuracy that the filter can achieve may be sufficient for many real spacecraft missions. Three-sigma accuracies on the order of 1500 m or smaller are predicted for LEO orbits with inclinations of 45 deg or more. These position accuracies depend on a number of factors. The sensor accuracies directly influence the result; the results assume a per-axis 1-σ magnetometer accuracy of 10 nT excluding biases and a 1-σ sun sensor accuracy of 0.005 deg. The spacecraft position accuracy degrades for inclinations below 45 deg. Accuracy also degrades as altitude increases.

A side benefit of the proposed system is increased accuracy of magnetometer-based attitude determination. The estimated corrections of the Earth's magnetic field model reduce the uncertainty in the inertial direction of this vector. Field direction accuracies on the order of 0.1 deg or better are predicted for the proposed system.

The proposed filter opens the possibility for a relatively inexpensive and effective combined attitude and orbit determination system. The only sensors would be a sun sensor and a magnetometer. The proposed system may be able to determine position to within 1.5 km and attitude to within 0.1 deg.

References

[1]Tapley, B. D., Ries, J. C., Davis, G. W., Eanes, R. J., Schutz, B. E., Shum, C. K., Watkins, M. M., Marshall, J. A., Nerem, R. S., Putney, B. H., Klosko, S. M., Luthcke, S. B., Pavlis, D., Williamson, R. G., and Zelensky, N. P., "Precision Orbit Determination for TOPEX/POSEIDON," *Journal of Geophysical Research*, Vol. 99, No. C12, 1994, pp. 24,383–24,404.

[2]Chory, M. A., Hoffman, D. D., and LeMay, J. L., "Satellite Autonomous Navigation—Status and History," *Proceedings of the IEEE Position, Location, and Navigation Symposium* (Las Vegas, NV), Inst. of Electrical and Electronics Engineering, New York, 1986, pp. 110–121.

[3]Tai, F., and Noerdlinger, P. D., "A Low Cost Autonomous Navigation System," *Proceedings of the Annual Rocky Mountain Guidance and Control Conference* (Keystone, CO), American Astronautical Society, San Diego, CA, Feb. 1989, pp. 3–23 (AAS Paper 89-001).

[4]Psiaki, M. L., and Martel, F., "Autonomous Magnetic Navigation for Earth Orbiting Spacecraft," *Proceedings of the 3rd Annual AIAA/USU Conference on Small Satellites* (Logan, UT), Utah State Univ., Logan, UT, 1989.

[5]Hicks, K. D., and Wiesel, W. E., Jr., "Autonomous Orbit Determination System for Earth Satellites," *Journal of Guidance, Control, and Dynamics*, Vol. 15, No. 3, 1992, pp. 562–566.

[6]Psiaki, M. L., Huang, L., and Fox, S. M., "Ground Tests of Magnetometer-Based Autonomous Navigation (MAGNAV) for Low-Earth-Orbiting Spacecraft," *Journal of Guidance, Control, and Dynamics*, Vol. 16, No. 1, 1993, pp. 206–214.

[7]Psiaki, M. L., "Autonomous Orbit and Magnetic Field Determination Using Magnetometer and Star Sensor Data," *Journal of Guidance, Control, and Dynamics*, Vol. 18, No. 3, 1995, pp. 584–592.

[8]Shorshi, G., and Bar-Itzhack, I. Y., "Satellite Autonomous Navigation Based on Magnetic Field Measurements," *Journal of Guidance, Control, and Dynamics*, Vol. 18, No. 4, 1995, pp. 843–850.

[9]Wiegand, M., "Autonomous Satellite Navigation via Kalman Filtering of Magnetometer Data," *Acta Astronautica*, Vol. 38, Nos. 4–8, 1996, pp. 395–403.

[10]Wu, S. C., Yunck, T. P., and Thornton, C. L., "Reduced-Dynamic Technique for Precise Orbit Determination of Low Earth Satellites," *Journal of Guidance, Control, and Dynamics*, Vol. 14, No. 1, 1991, pp. 24–30.

[11]Langel, R. A., "The Main Field," *Geomagnetism*, edited by J. A. Jacobs, Vol. 1, Academic, New York, 1987, pp. 249–512.

[12]Gill, P. E., Murray, W., and Wright, M. H., *Practical Optimization*, Academic, New York, 1981.

[13]Kailath, T., *Linear Systems*, Prentice–Hall, Englewood Cliffs, NJ, 1980, pp. 615–618.

[14]Psiaki, M. L., Theiler, J., Bloch, J., Ryan, S., Dill, R. W., and Warner, R. E., "ALEXIS Spacecraft Attitude Reconstruction with Thermal/Flexible Motions Due to Launch Damage," *Journal of Guidance, Control, and Dynamics*, Vol. 20, No. 5, 1997, pp. 1033–1041.